An integrated magnetotelluric study of the Mt. Etna volcanic structure

Paolo Mauriello ([1]), **Domenico Patella** ([2]), **Zaccaria Petrillo** ([3]) and **Agata Siniscalchi** ([4])

([1]) *Istituto per le Tecnologie Applicate ai Beni Culturali, CNR, Roma, Italy*

([2]) *Dipartimento di Scienze Fisiche, Università «Federico II», Napoli, Italy*

([3]) *Osservatorio Vesuviano, Ercolano, Napoli, Italy*

([4]) *Dipartimento di Geologia e Geofisica, Università di Bari, Italy*

Abstract

The results of a magnetotelluric (MT) survey performed at Mt. Etna (Sicily, Italy) are presented and discussed. The MT interpretation is preceded by the description of the data managing strategy used for the estimate of the impedance tensor and the computation of a rotationally invariant parameter. The 1D Bostick inversion of MT soundings located in the Etnean central area highlights the existence of a wide conductive zone in the depth range 15-30 km. Resistivities of a few $\Omega \cdot$ m are estimated in the southern part of this zone, while resistivities one order of magnitude higher are estimated in the northern part. In the central sector, the MT soundings are characterized by much higher resistivity values suggesting the presence of an E-W directed resistive barrier separating the two conductive deep zones. A two-feeding system is thus hypothesized as an extension of a previous 3D model deduced from regional earthquakes and teleseisms in the depth range 15-25 km. Moreover, the comparison with previous shallow seismic tomographies from local earthquakes within the first 11 km of depth allows us to distinguish inside the upper portion of the resistive barrier a central high velocity zone. This zone can likely be ascribed to a slowly cooled dike tending to become highly fractured at its western and eastern edges. Finally, the impedivity analysis based on the comparison with previous geoelectric dipole soundings allows us to exclude the existence of a permanent magma chamber within the first 5 km of depth and to argue the existence of a shallow plumbing system consisting of a medium-to-low temperature hydrothermally altered environment.

Key words *magnetotellurics – Mt. Etna – volcanic structure – feeding system*

1. Introduction

The study and control of the dynamics of an active volcano is largely facilitated by the knowledge of the structural setting of its feeding and plumbing systems. To this purpose, the geophysical contribution has long demonstrated its importance everywhere. In particular, the magnetotelluric (MT) method is most advantageous as it determines the deep crustal distribution of the electric resistivity, which is a highly diagnostic parameter in volcanic areas. The MT method permits also to draw complex resistivity (impedivity) shallow signatures because of the close dependence of the EM field pattern on temperature and rock-fluid interaction phenomena typical of active systems.

In this paper, we outline a structural interpretation of the central part of Mt. Etna (Sicily, Italy), obtained from a set of MT soundings extended over a wide period band from about 0.004 s to 1000 s. A local 1D modelling was

Mailing address: Dr. Paolo Mauriello, Istituto per le Tecnologie Applicate ai Beni Culturali, CNR, Via Salaria km 29,300, 00016 Monterotondo St., Roma, Italy; e-mail: mauri@na.infn.it

attempted, taking care of the limitations of such an approach when it is applied to an actual 3D environment.

The MT stations were located close to previous deep dipole electrical sounding centres (DES) (Loddo *et al.*, 1989). The integration of MT and DES data makes possible: a) to solve static shift effects on the MT sounding curves (Zhdanov and Keller, 1994); b) to set an optimal procedure for impedance estimate in high frequency acquisition ranges (Giammetti *et al.*, 1996; Di Maio *et al.*, 1998; Mauriello *et al.*, 1997); c) to dispose of shallow layer resistivity and depth constraints in MT interpretation (Vozoff and Jupp, 1975; Coppola *et al.*, 1993); d) to single out resistivity frequency dispersion effects (impedivity analysis) (Patella, 1987, 1993; Patella *et al.*, 1991; Mauriello *et al.*, 1996).

To improve the knowledge of the Mt. Etna volcanic structure, we compared our MT interpretation with the seismic model suggested by Sharp *et al.* (1980), who studied travel time

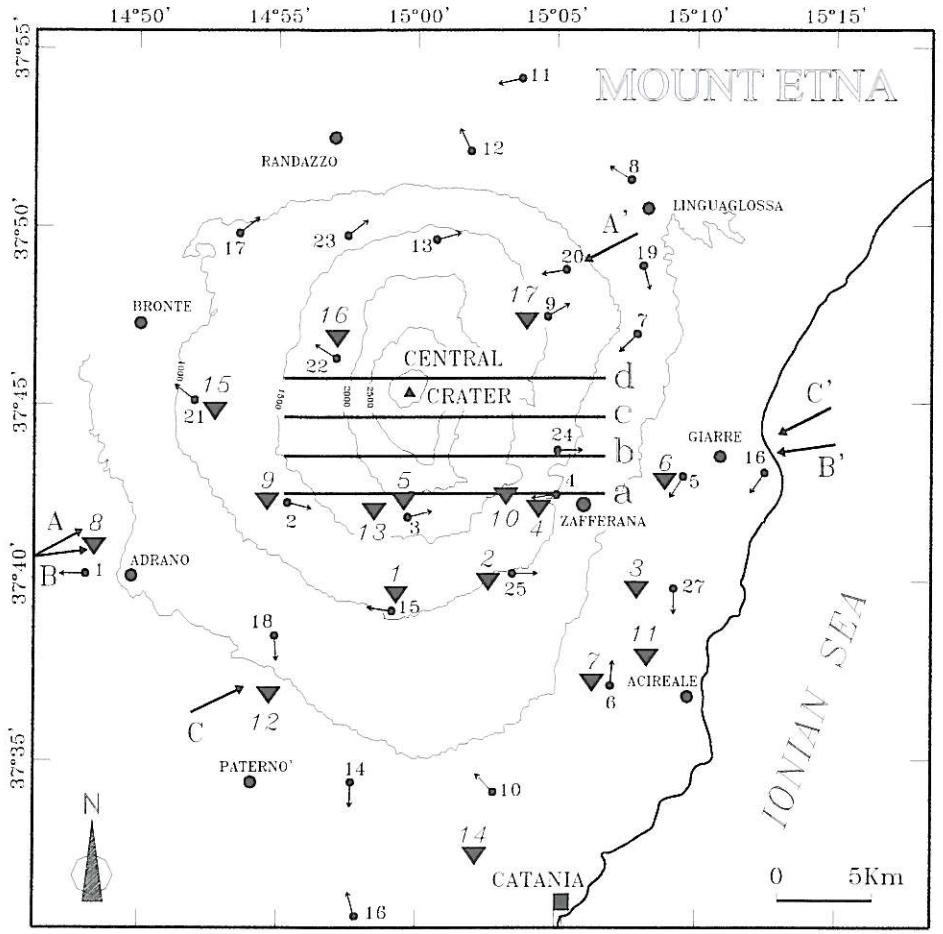

Fig. 1. Location map of the magnetotelluric (triangles) and deep dipole geoelectrical (dots with arrows) sounding stations, the tomographic seismic profiles (heavy lines *a*, *b*, *c*, *d*) and the MT transects AA′, BB′ and CC′ at the Mt. Etna volcanic area.

inversions from a set of regional earthquakes and teleseisms, and with the tomographies elaborated by Hirn *et al.* (1991), who analysed *P* and *S*-wave arrivals from regional and local earthquakes and artificial sources.

Figure 1 shows the location map of all the geophysical surveys performed in the Etnean area, which are considered in this paper.

2. Geological background

Mt. Etna is situated in the eastern part of Sicily (Italy). It is the largest and most active volcano in Europe. It formed about a zone of complex geodynamics, which is thought to be related to the subduction of the African Plate beneath the Eurasian Plate (Barberi *et al.*, 1973). The tectonic complexity of the zone is also confirmed by the different activity styles shown by the volcanoes developed in this area of Southern Italy. The calc-alkaline products of the Eolian volcanic arc, located about 100 km to the north from Etna, are likely to be associated with a compression zone (Northern Sicily suture zone), whereas the prevailing basaltic products of Mt. Etna would be related to an extension zone.

The structural units that characterise Eastern Sicily are from south to north the Iblean Foreland, the Gela-Catania Foredeep, the Caltanissetta Trough and the Northern Chain. Following Lentini (1982), the essential tectonic pattern is that the Iblean Foreland, *i.e.* the Sicilian margin of the African Plate, would have been affected by downfaulting that produced the Caltanissetta Trough, the southeastern part of which is referred to as the Gela-Catania Foredeep. The Northern Chain is considered a fragment of the Apenninian-Maghrebian Chain. It consists of nappes that progressively thrust over one another and finally slid into the Caltanissetta Basin (Scandone *et al.* 1977).

Mt. Etna is located between the Iblean Plateau and the Northern Chain and its volcanism is thought to have been activated by trends cutting almost transversally the main foredeep-foreland system on the Ionian side. Figure 2 shows a schematic picture of the tectonic outline of Eastern Sicily.

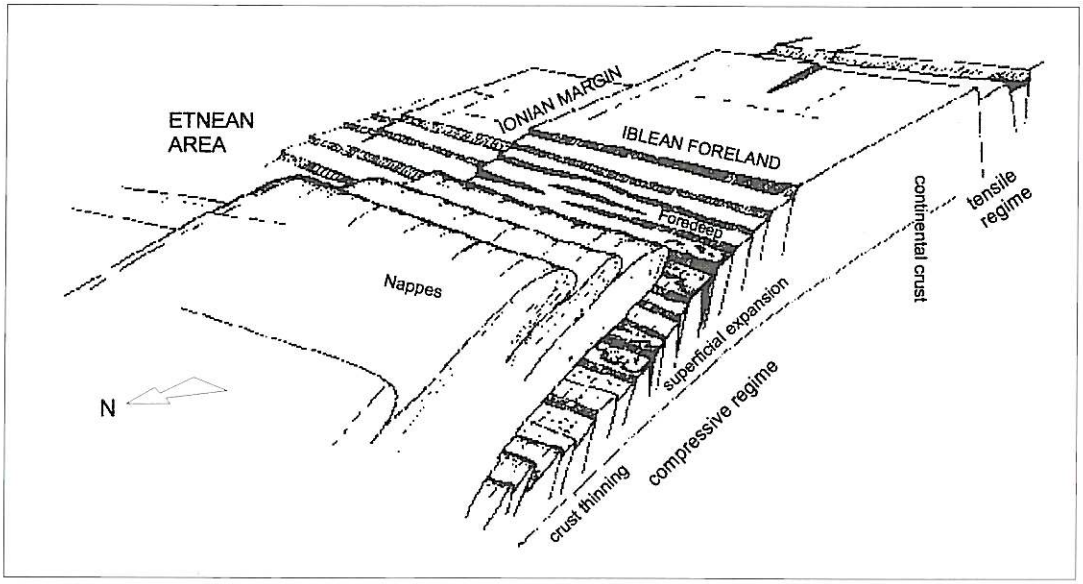

Fig. 2. Schematic tectonic picture of Eastern Sicily (redrawn after Lentini, 1982).

3. The magnetotelluric study

Before showing the MT results obtained in the Etnean area, we outline the strategy pursued to process and represent the data, since the application of MT in volcanic areas is not as usual as it is in the study of a sedimentary basin.

3.1. *MT data managing strategy*

In the Etnean area the data were sampled within the frequency bands $5 \cdot 10^{-4}$ Hz-0.25 Hz, 10^{-2} Hz-2.5 Hz, 0.2 Hz-50 Hz and 1 Hz-250 Hz.

To control the influence of noise on the MT sounding data, the two impedance estimates including the autopowers of the magnetic and electric field components were made respectively (Sims *et al.*, 1971; Vozoff, 1972). In principle, the two procedures give identical results in absence of noise. However, if an uncorrelated noise is present and the records are processed as if they were noise-free, downward and upward biased impedance estimates are obtained using the first and the second procedures, respectively.

Almost all MT soundings showed the presence of mis-tie effects in the overlapping region 0.2-2.5 Hz between the second and the third frequency bands. Mis-tie effects could be readily removed using the second impedance estimate procedure for the two lower frequency bands and the first procedure for the two higher frequency bands.

The standard skew parameter (Swift, 1967) was then calculated and values much greater than 0 were obtained for all soundings in the whole frequency range. This result prevented us from assuming a unique background regional strike within the whole survey area. Thus, we decided to compute a set of MT apparent resistivity diagrams, rotated at each frequency to the two principal axes along which the antidiagonal impedance elements took on their largest and smallest values, respectively (Vozoff, 1972).

The comparison of most of these last MT apparent resistivity estimates with the common station DES data showed high mutual consistency, which proved the reliability of the strategy used to eliminate mis-tie effects. Only in a few cases, as in soundings MT1 and MT9 to a greater extent, was this consistency not observed and upward static shift effects were inferred. Each static shift effect was eliminated by shifting downward the perturbed MT curve until it matched the nearest DES curve.

We therefore conclude that in general an uncorrelated random noise affected the magnetic field components within the low frequency bands, while it prevailed in the electric channels at high frequencies. Figure 3 shows the antidiagonal apparent resistivity diagrams, for which an MT-to-DES adjustment was made as discussed above.

The interpretation of MT data collected in volcanic areas is a difficult task and the question of which method is more appropriate to find a reliable solution is still a matter of debate. In principle, a volcano is a complex 3D structure, but 3D modelling requires such a large data set and *a priori* boundary constraints that a rigorous solution can hardly be achieved. This is mainly true for Mt. Etna, where the huge dimension of the volcanic apparatus and the wide extension of inaccessible sites do not permit us to dispose of a large dense grid of MT stations. Neither do the conditions exist for a 2D modelling of the 3D structure following Wannamaker *et al.* (1984), since our MT data do not show a prevailing strike direction, as previously outlined.

1D reliable modelling can instead be attempted favoured by the previously discussed MT-to-DES adjustment strategy (Hördt *et al.*, 1992; Kellett *et al.*, 1992; Parker and Booker, 1996). In considering such an attractive opportunity, Wannamaker *et al.* (1984) pointed out that misleading interpretations could only be obtained if the simplified 1D approach were applied to MT soundings located over a laterally bounded, conductive and relatively shallow layer (a few $\Omega \cdot$ m at a few kilometres of depth). In fact, because of the strong persistence of induced charge accumulations over the vertical boundary planes, the MT apparent resistivity curves are affected from the beginning by a downdipping asymptotic distortion that has no relationship with the underlying structures, which cannot consequently be identified. The MT curves of fig. 3 indeed reveal in the central part of the surveyed area the presence of a conductive layer, which appears

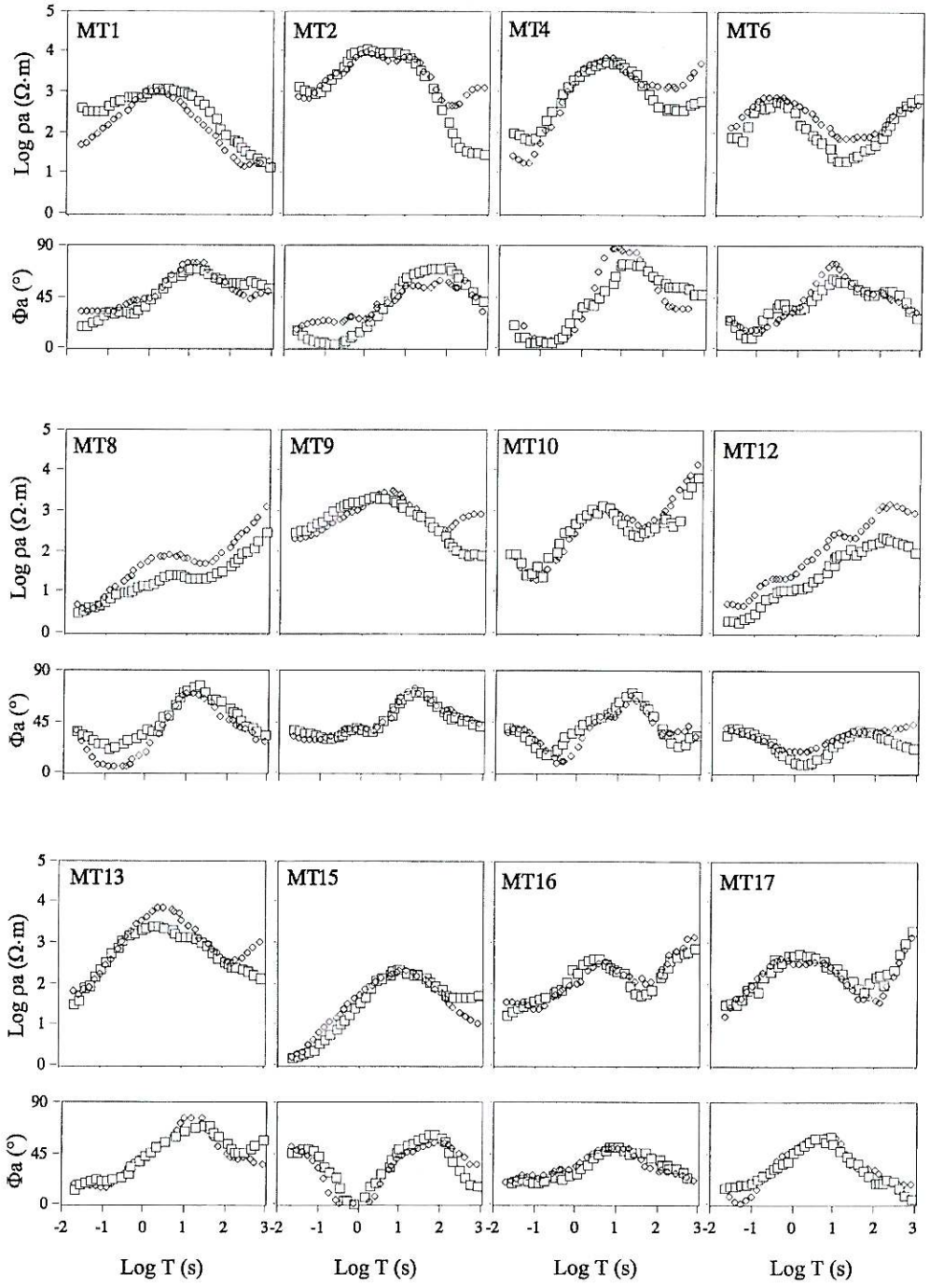

Fig. 3. Magnetotelluric rotated apparent resistivity diagrams in the TM (lozenges) and TE (squares) modes.

however located within a very great skin-depth interval, of the order of a few tens of kilometres. Accordingly, the distortion effect if present would be notably scaled down and thus be irrelevant for the purposes of our study.

Ingham (1988) suggests that the MT curves derived from rotationally invariant parameters can be used for a 1D analysis of a 3D structure without incurring the risk of misinterpretation that seriously afflicts the modelling of the conventional polarization modes. Assuming such a point of view, we derived the apparent resistivity values from the determinant of the impedance tensor matrix as follows (Ranganayaki, 1984)

$$\rho_{\mathrm{Det}} = \frac{1}{\omega\mu_0}\left|\det \mathbf{Z}\right| = \frac{1}{\omega\mu_0}\left|Z_{xx}Z_{yy} - Z_{xy}Z_{yx}\right|, \tag{3.1}$$

where μ_0 is the magnetic permeability of free space, ω is the angular frequency and Z_{uv} ($u, v = x, y$) is the generic element of the $\mathbf{Z}$ matrix.

Among all known invariants, the determinant is in a sense an average impedance. Park and Livelybrooks (1989) and Ingham (1992) maintain that the use of an invariant impedance may provide a simple, relatively accurate tool for interpreting MT data even in 3D areas. Again, only in the presence of a relatively shallow strong inhomogeneity can this approach potentially lead to some radical misinterpretation of the deeper structures. However, since we are interested in identifying the presence of deep conductors as far as a few tens of kilometres without attempting to resolve underlying structures, the above limitation is indeed rather ineffective.

Accounting for the above discussion, we finally decided to make recourse to Bostick's 1D inversion algorithm (Bostick, 1977; Torres-Verdín and Bostick, 1992). As stated in very recent papers (Nagy, 1996; Zhdanov *et al.*, 1996), Bostick's method is currently accepted as the most suitable transformation of the apparent resistivity curve in the 1D domain. Indeed, Bostick's method generates continuous resistivity-*versus*-depth profiles not constrained by sharp discontinuities (Weaver and Agarwal, 1993), whose depth location is in principle uncertain due to equivalence. This is particularly true in complex volcanic areas, where generally it is not possible either to perform extended MT surveys or to dispose of borehole-controlled boundaries. Bostick's inversion is based on the following algorithm:

$$\rho(z) \cong \left[\frac{d}{dz}\frac{z}{\rho_{\mathrm{Det}}}\right]^{-1} = \rho_{\mathrm{Det}}\frac{2+m}{2-m}, \tag{3.2}$$

where

$$m = \frac{d\log\rho_{\mathrm{Det}}}{d\log\sqrt{T}}. \tag{3.3}$$

In eq. (3.2), z is the pseudodepth, equal to $\sqrt{\rho_{\mathrm{Det}}T/\omega\mu_0}$, where T is the period.

3.2. *MT data representation*

In order to obtain a reliable picture of the electrical resistivity distribution in the Etnean area, we selected the best set of processed MT soundings, corresponding to 12 stations all located in the central sector of the volcanic area. A frequency-slice representation was adopted to highlight a correlation among soundings.

Figure 4a-h shows seven frequency-slices computed at seven frequencies logarithmically equally spaced over the whole data acquisition frequency range. Each slice from fig. 4b to fig. 4h represents a contour plan view of the values of ρ_{Det} computed using eq. (3.1) and attributed to the corresponding MT stations, whose location is given in fig. 4a. Due to the poorly dense grid of the MT stations, each slice representation gives only a smooth distribution pattern of the determinant apparent resistivity at a given frequency. Nevertheless, a roughly E-W elongated resistive structure seems to prevail in the frequency range from 1 to about 10^{-2} Hz.

For the comparison between MT and DES data, an MT synthetic response was calculated on the basis of the DES 1D interpretation given by Loddo *et al.* (1989). 13 DES close to the MT sites were taken into account. Figure 5a-d shows the frequency-slices of the synthetic MT re-

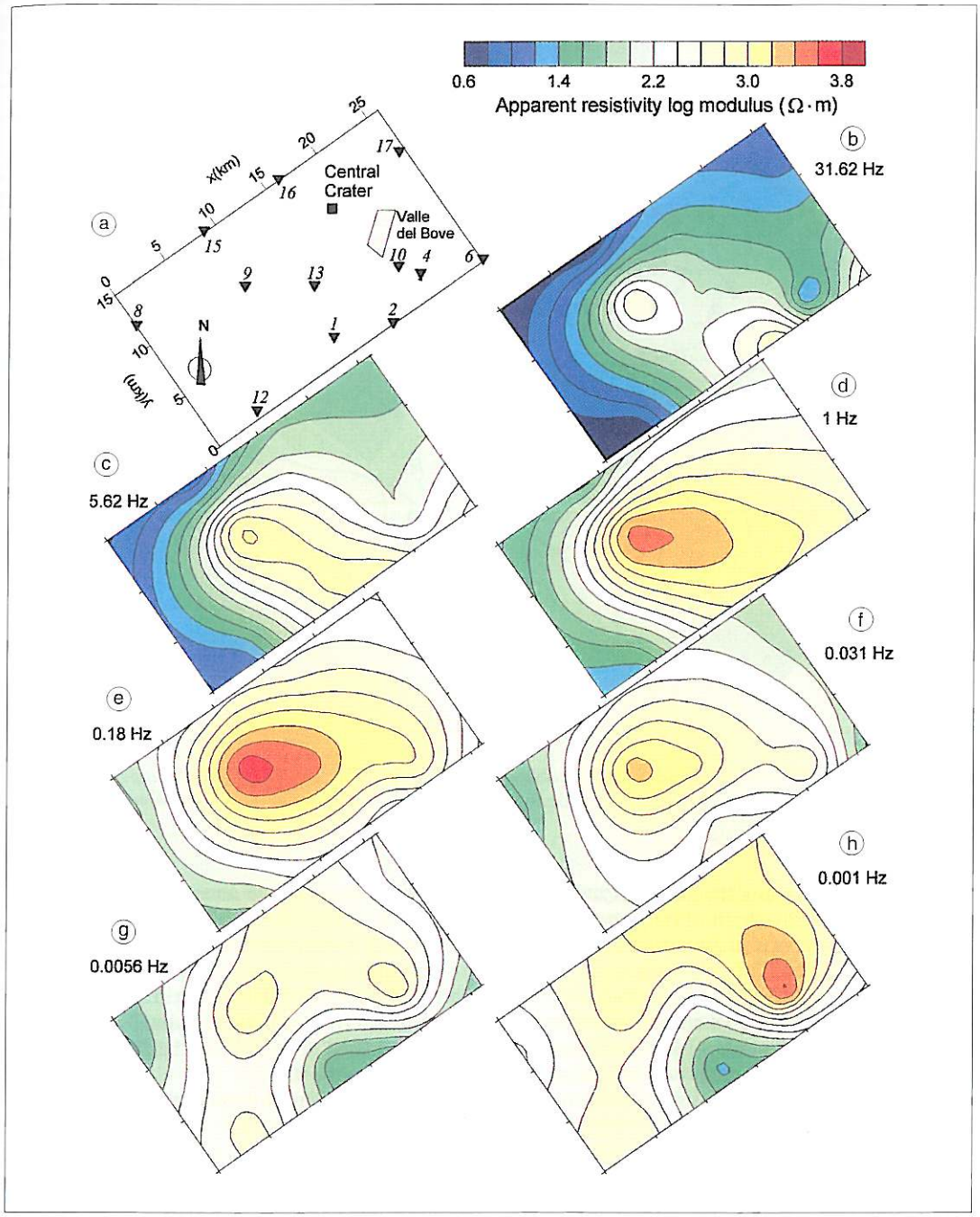

Fig. 4a-h. Magnetotelluric data representation: a) MT stations location map; b) through h) horizontal frequency slices of the modulus of the determinant apparent resistivity.

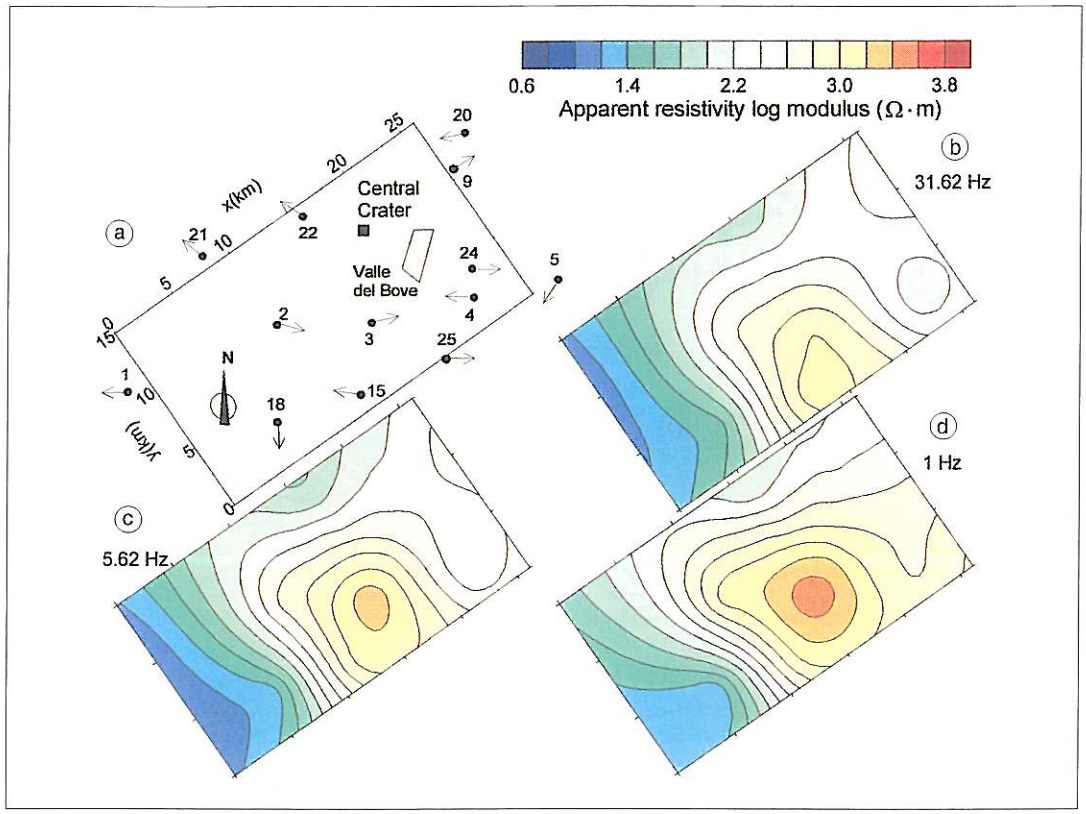

Fig. 5a-d. Synthetic MT data representation, obtained by the deep Dipole Geoelectrical Soundings (DES). a) The DES stations location map; b,c,d) as in fig. 4.

sponses computed using the geoelectrical models. Only the first three highest frequencies were used for the comparison because of the DES notably smaller depth of penetration.

We observe large scale comparable patterns of the two determinant apparent resistivity contoured estimates. To make a likelihood test between the two sets of frequency-slices, we introduce a percent MT-DES discrepancy factor $E_{\%}(x, y)$ as follows:

$$E_{\%}(x,y) = 100\,\frac{\log \rho_{\mathrm{Det}}^{\mathrm{DES}}(x,y) - \log \rho_{\mathrm{Det}}(x,y)}{\log \rho_{\mathrm{Det}}(x,y)}, \tag{3.4}$$

where $\rho_{\mathrm{Det}}(x, y)$ is the actual MT determinant apparent resistivity and $\rho_{\mathrm{Det}}^{\mathrm{DES}}(x, y)$ is the equivalent quantity reconstructed from the DES data.

Each slice of fig. 6a-d represents a contour map of $E_{\%}(x, y)$. Considering that the average statistical error in both MT and DES surveys was estimated around 10%, the following conclusions can be drawn:

1) Low values of the logarithmic discrepancy ($|E_{\%}| \leq 20$) in slices *b*, *c* and *d* are taken as representative of an overall good agreement between MT and DES data.

2) High positive values ($E_{\%} > 20$) in slice *b*, in correspondence of the Valle del Bove (see slice *a*), in the central part, as well as in the northern and southern parts, are instead assumed

Fig. 6a-d. The Percent Discrepancy Parameter (PDP) representation. a) The MT and DES stations location map; b,c,d) the PDP horizontal frequency slices.

to indicate the presence of resistivity dispersion effects in the shallower zones.

The major concern is of course devoted to the second statement for its great implication in volcanology. This topic will be extensively dealt with in a following section.

3.3. *MT structural interpretation*

Figure 7a-c shows the true resistivity cross sections obtained by the 1D Bostick inversion along the profiles AA′, BB′ and CC′, whose traces are drawn in fig. 1. A reliability test was performed using the maximum error propagation rule, which allowed us to conclude that the resistivity-*versus*-depth general pattern drawn in the contoured sections of fig. 7a-c remains substantially uneffected by unavoidable local random errors.

It is now worth observing that the Mt. Etna complex is surrounded by the two main conductors outcropping in the whole area, namely the Caltanissetta Basin to the west and the Ionian Sea to the east. Hence, the resistivity-depth images at the edges of the sections must be taken with some care as we cannot in principle exclude some distorting lateral effects. This is mainly true for soundings MT6 and MT8 located at the border of the volcanic massif.

Both profiles AA′ and CC′ clearly show the presence of wide conductive zones. The lowest

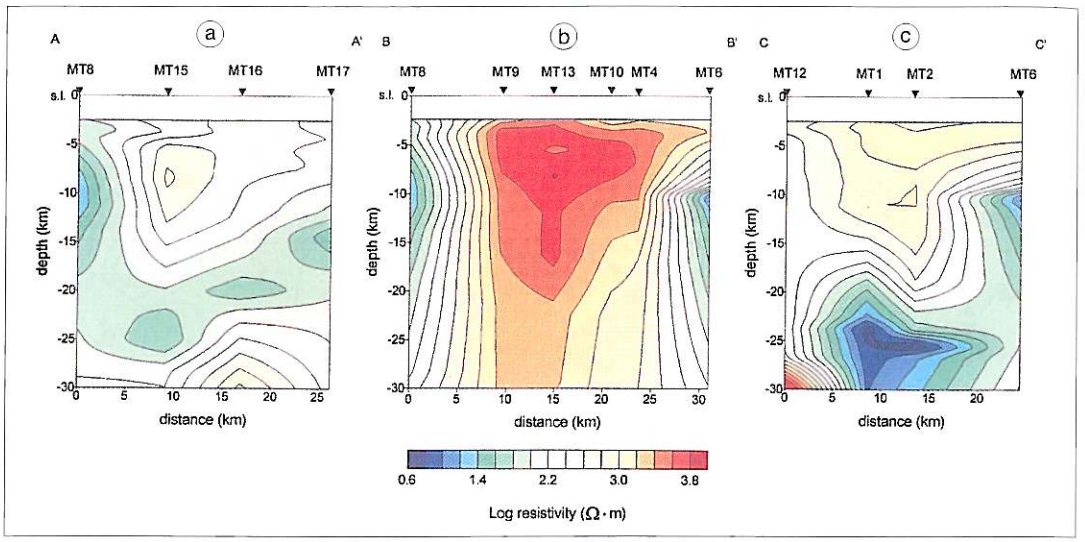

Fig. 7a-c. MT 1D Bostick inversion for the profiles AA′ (a), BB′ (b) and CC′ (c) of fig. 1.

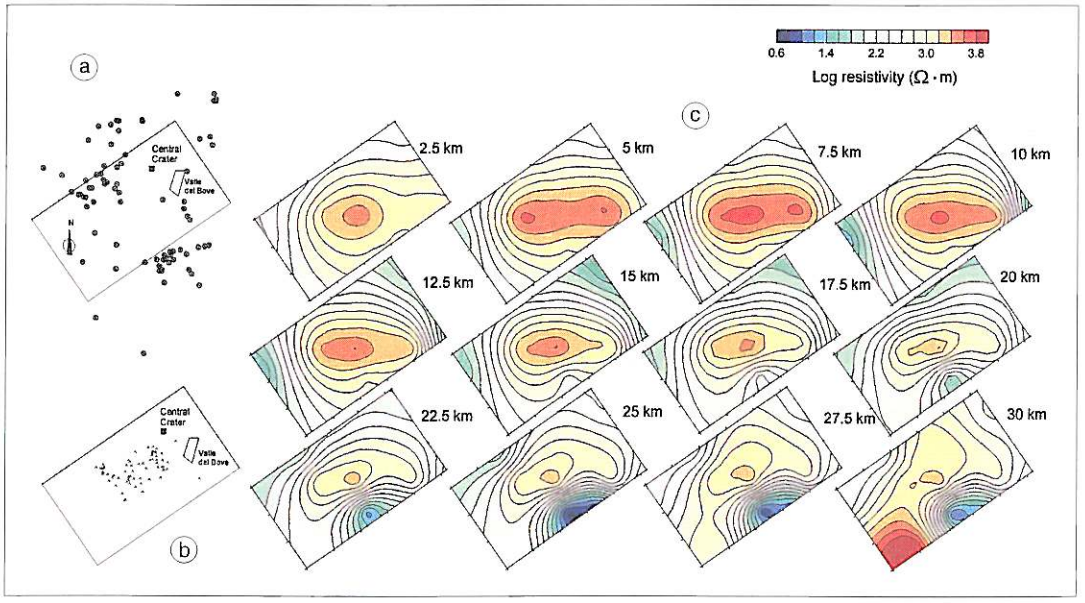

Fig. 8a-c. a) Location map of the eccentric cones (redrawn after Rittmann, 1973); b) location map of the earthquake epicentres (redrawn after Patanè *et al.*, 1994); c) sequence of twelve horizontal resistivity-*versus*-depth slices in the interval 2.5-30 km.

resistivity values were met across the southernmost CC′ profile. In particular, the local minimum in the profile AA′ reaches about 30-40 Ω·m, while in the profile CC′ it drops to about 3-4 Ω·m. Generally speaking, we estimate that the whole conductive zone in profile AA′ is one order of magnitude less conductive than that in profile CC′. Such a bipartition also seems supported by the presence of a large central resistive barrier across the profile BB′, deepening at least down to 30 km.

The above electrical picture can be related to the volcanic and seismological pattern of Mt. Etna (fig. 8a-c).

As concerns the first aspect, the localisation of the deep conductors well correlates with the surface distribution of the eccentric volcanoes. Figure 8a, which shows the *adventive* cones map after Rittmann (1973, fig. 2), is compared with fig. 8c, where a sequence of twelve MT horizontal depth slices in the interval 2.5-30 km below the Etnean area is depicted. In the southern part of the slices, starting from 20 km downward, the highly conductive zone beneath MT1 and MT2 closely corresponds to the southernmost dense cluster of eccentric volcanoes. A similar correlation can also be observed between the conductive zone in the northern part of the slices and the northernmost distribution of *adventive* cones. In the central part of the area, in correspondence with the highly resistive body, Rittmann's classification includes only lateral eruptive centres and eruptive radial fissures.

As concerns the second aspect, it is widely accepted that the background seismotectonic activity at Mt. Etna is normally concentrated around the central area (see *e.g.*, the epicentre map of Cosentino *et al.*, 1982). Referring to the most recent and best monitored seismic activity in the central area before the 1991-1993 eruption (Patanè *et al.*, 1994; Bonaccorso *et al.*, 1996), which was the largest in this century, we observe that the epicentres distribution drawn in fig. 8b closely corresponds to the highly resistive body image. The correlation is also well evident if we consider the depth distribution of the hypocentres. Figure 9, in fact, shows again the 1D Bostick inverted BB′ section, across which the earthquake hypocentres, relative to

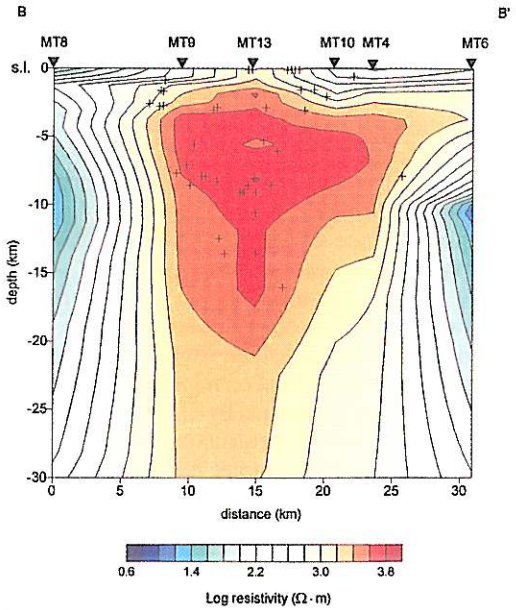

Fig. 9. MT 1D Bostick inversion for the profile BB′ with localization of the earthquake hypocentres (redrawn after Patanè *et al.*, 1994).

the early part of 1991 (after Patanè *et al.*, 1994), are reported. The high-resistivity zone closely coincides with the volume in which the most part of the seismic energy was released.

At present, the large scale picture hereabove discussed seems to be the most relevant electrical contribution to the understanding of the volcanic system and of its roots at great depth.

4. Electrical resistivity *versus* seismic velocity

The relationship between resistivity and seismic velocity is not quite so simple. In general, in active volcanic areas the presence of some percent of molten rock is expected to produce a decrease of both resistivity and velocity. The same effect can also be ascribed to the presence of wet fractured volcanics. We refer to these situations as $L_\rho L_v$ zones. A resistivity low related to a velocity high would be instead expected in zones of intense hydrothermal alteration with

abundant mineral particles deposition. We refer to this second situation as to the $L_\rho H_v$ zone. Conversely, a resistivity high related to a velocity low could be characteristic of highly fractured and dry volcanics. We refer to this third situation as to the $H_\rho L_v$ zone. Finally, a resistivity high correlated with a velocity high would be the response of dry and compact volcanics, like for instance slowly cooled dikes. We refer to this last situation as to the $H_\rho H_v$ zone.

A way to test all such possibilities in the Etnean area was to compare our MT data with previous seismic data. The seismic study of residual travel times based on regional earthquakes and teleseisms, performed by Sharp *et al.* (1980), was used for the deeper structure of the volcano and the seismic tomography, elaborated by Hirn *et al.* (1991) using *P* and *S* arrivals from local earthquakes, for the shallower part.

4.1. *Magnetotellurics compared with regional seismics*

As pointed out by Sharp in his review on deep seismic sounding at Mt. Etna (1982), the most striking common feature of the different crustal models proposed in previous papers (Cassinis *et al.*, 1969; Colombi *et al.*, 1979; Sharp *et al.*, 1980) is a large low velocity layer of 5.5-6.0 km/s in the depth range 15-25 km. In particular, Sharp *et al.* (1980), using a 2D array and computation of travel time residuals from regional earthquakes and teleseisms, modelled a three-axial north-northeastward trending ellipsoid at an average depth of 20 km, as shown in fig. 10. The computed velocity reduction of about 16% in the ellipsoid was interpreted as evidence of a not completely molten magma chamber or rather a complex network of veins of melt running through the ellipsoidal body.

Although $L_\rho L_v$ zones occur in about the same depth range, the comparison between the depth slices reported in fig. 8c, limited to the depth interval 15-25 km, and Sharp *et al.*'s (1980) model, redrawn in fig. 10, shows that the observed large scale geometry of the low resistivity zones does not conform to a totally uniform ellipsoid-like magma chamber or vein network, at least in the central part of the seismic ellipsoid. The presence of the roughly E-W elongated resistive barrier and the different order of magnitude of the resistivity to north and south of the resistive dike-like body would rather suggest the existence of a two-feeding volcanic system. The following discussion aims at giving some more insight into this possibility.

Shankland and Ander (1983) maintain that deep crustal conductive zones have conductivities closely dependent on ionised fluids amount, temperature and partial melt percentage. They correlated the high conductivity with the regional heat flow measured in different regions of complex tectonics all over the globe and were able to infer roughly linear log conductivity-*versus*-temperature empirical diagrams of direct proportionality. The empirical correlations appear convincingly clustered about three general trends, respectively associated with the Low Conductive Layer (LCL) in regions of stable platform, the LCL in regions of recent tectonic activity and to the High Conductivity Layer (HCL) in both regions.

This result enabled us to make a temperature estimate inside the two HCL evidenced in the Etnean area. Therefore, referring to Shankland and Ander's (1983) unified conductivity-*versus*-temperature empirical diagram (the authors' fig. 6), opportunely bounded by Olhoeft's (1981) laboratory similar diagrams for wet and dry volcanics, we tentatively estimate for the Etna volcano an average temperature not greater than 600 °C to the north and about 1000 °C or more to the south within the respective conductive deep zones.

As pointed out by Shankland and Ander (1983), estimated temperatures over 1000 °C, substantially higher than solidus temperatures, are outside the range of validity of purely conductive heat flow. In tectonic regions this circumstance is a strong argument for the existence of partially molten bodies. Moreover, partial melting in the low-velocity zone, where it exists, is highly probable if this region of seismic velocity retardation and attenuation is accompanied by a marked increase in the electrical conductivity (Waff 1974; Shankland *et al.*, 1981).

We may thus infer that at least the southern conductor can be interpreted as a partially mol-

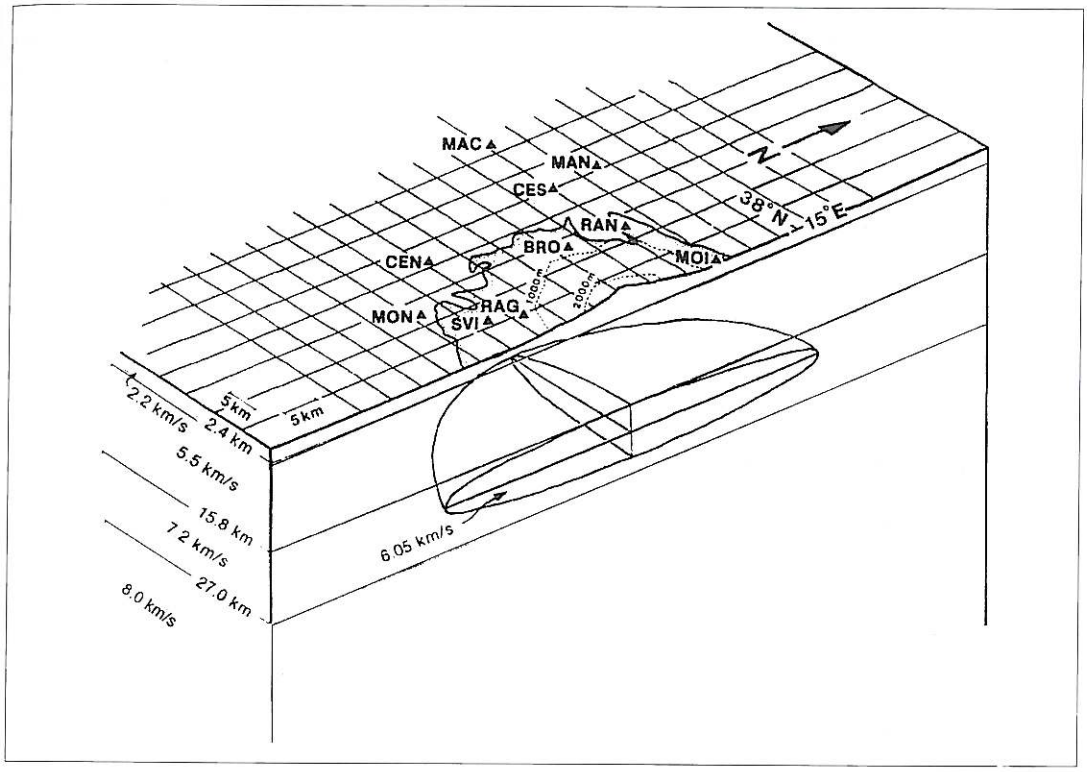

Fig. 10. A schematic crustal model and low velocity anomaly beneath Mt. Etna volcano (redrawn after Sharp, 1982).

ten body. This conclusion is also supported by geochemical data indicating that eruptions in the past three millennia were fed largely by trachybasaltic magmas coming from the deep, permanent subcrustal reservoir in the 20-30 km depth range (Condomines *et al.*, 1982; Tanguy *et al.*, 1997).

A tentative estimate of the melt fraction can also be made following Waff's theoretical model (Waff, 1974) for continuous grain boundary wetting. Assuming a resistivity of the liquid phase at 1200°C for tholeitic basalt of around 0.3 $\Omega \cdot$m and our estimated resistivity of 3-4 $\Omega \cdot$m for the bulk conductive body, a melt fraction of about 12-16% is obtained. Also this estimate is in good agreement with Tanguy *et al.*'s (1997) conclusion.

4.2. *Magnetotellurics compared with local seismics*

For the study of the shallow structures, the only seismic and MT lines which can be considered almost coincident are the MT BB′ transect and Hirn *et al.*'s *a* and *b* seismic profiles, sketched in fig. 1. Figure 11a-d shows the comparison between the results from the local seismic tomography and the 1D Bostick-inverted MT data. The pictures are true vertical sections with the depth scale ranging from about the volcano free surface down to 8 km. The top section in fig. 11a shows the resistivity distribution with the darker grey palettes indicating low resistivities and the lighter grey ones high resistivities. Accordingly, the two following sections in

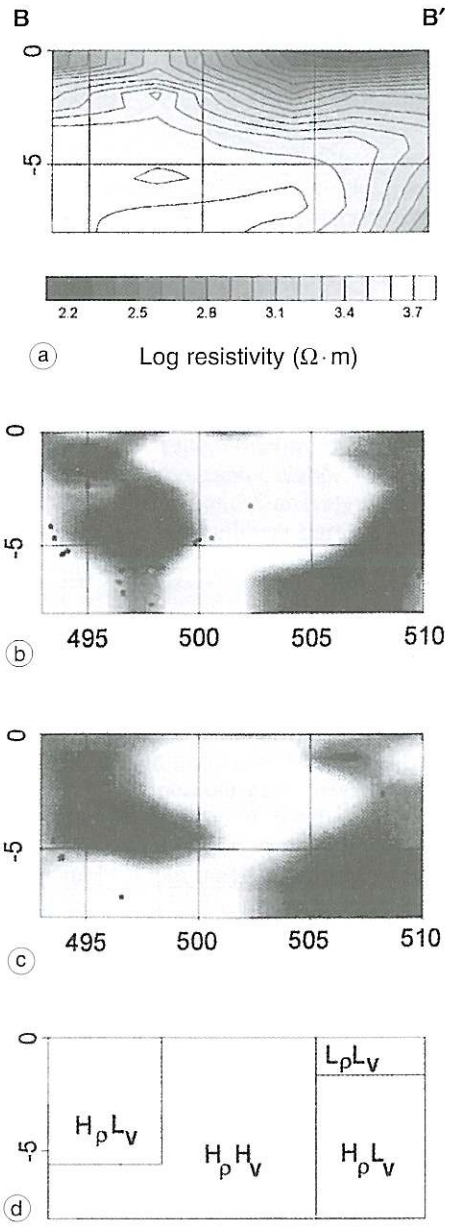

Fig. 11a-d. Comparison between MT true resistivity section and local seismic tomographies. a) The MT 1D Bostick inversion along profile BB′ of fig. 1; b,c) seismic tomographies of *P* velocity deviation along profiles *b* and *a* of fig. 1, respectively (redrawn after Hirn *et al.*, 1991, fig. 4); d) volcanically interpreted section.

fig. 11b,c show the velocity distribution along Hirn *et al.*'s *b* and *a* profiles, respectively, with dark grey indicating low velocities and light grey high velocities.

From a qualitative point of view the comparison between the MT and the local seismic tomography displays the following features, which are also synthesised in the bottom section of fig. 11d, where, for the sake of simplicity, a few straight segments are drawn to indicate the boundaries of the most relevant zones.

a) On the eastern part of the section, which corresponds to the Valle del Bove southeastern border, a resistivity high correlates with a velocity low at the bottom. The agreement seems well defined even from the geometrical point of view. Dry fractured volcanics would be there ascribed ($H_\rho L_v$ zone). In the upper part of the same region an $L_\rho L_v$ zone seems to exist, which can be ascribed to the presence of wet fractured volcanics. This hypothesis is also supported by the occurrence of the resistivity dispersion effects mentioned in Section 3.2., which will be discussed in more detail in the next section.

b) On the central part of the section a resistivity high correlates with a velocity high. Slowly cooled compact dikes would there correspond ($H_\rho H_v$ zone).

c) On the upper part of the western zone of the section a resistivity high correlates again with a velocity low. Again, dry fractured volcanics would be there associated ($H_\rho L_v$ zone). The lower part is rather ambiguous, even though an $H_\rho H_v$ zone seems to prevail. Indeed, it must be mentioned that in this zone the seismic profile *a* is the least resolved by the ray-tracing tomography, because of the lack of an adequate seismic stations coverage, while a much denser station array was done in the left-hand side of profile *b* (Hirn *et al.*, 1991).

The comparison between the MT profile BB′ and the nearest shallow seismic tomography singles out a slowly cooled compact dikes zone, surrounded by very likely fractured volcanics with alteration phenomena mainly concentrated in the upper eastern side.

Table I. Combined MT-DES interpretation to single out dispersive layers by Cole-Cole modelling. In sequence, the columns report the zero-frequency resistivity of the layers, the corresponding thickness, the Cole-Cole principal time constant, the chargeability and the frequency factor.

Sounding	$\rho_i(\Omega \cdot m)$	$h_i(m)$	$\tau(s)$	m	c
	8000	80	0.02	0.99	0.68
MT-1	2100	260	90	0.97	0.63
	1000				
	4500	100			
	4500	100	15	0.99	0.6
MT-2	650	700			
	650	2100			
	1000				
	3200	50	0.9	0.999	0.4
MT-4	130	150	15	0.98	0.55
	130	1510			
	30000				
	135	63	0.1	0.999	0.63
MT-8	5.6	300			
	500				
	1500	10			
	10000	40			
MT-10	600	460	9	0.93	0.6
	600	1200			
	10000				
	1300	145	1	0.999	0.6
	15	100	10	0.9	0.6
MT-12	15	1400			
	1000				
	1600	780	20	0.997	0.6
MT-13	500	800			
	10000				
	8000	45			
	2100	230	250	0.9999	0.66
MT-15	18	120	80	0.999	0.16
	18	60			
	350				
	7200	330	100	0.999	0.24
MT-16	25	50	2.5	0.999	0.38
	25	500			
	300				
	500	25	1	0.99	0.6
MT-17	2000	400			
	250	100	40	0.995	0.56
	250				